Original Article

Journal of LOW FREQUENCY NOISE, VIBRATION AND ACTIVE CONTROL

Journal of Low Frequency Noise, Vibration and Active Control
0(0) 1–13

DOI: 10.1177/0263092317716075
journals.sagepub.com/home/lfn
SAGE

Detection and control of a gyroscopically induced vibration to improve the balance of a single-wheel robot

Sangdeok Lee and Seul Jung

Abstract

In this article, an experimental investigation of the detection of a gyroscopically induced vibration and the balancing control performance of a single-wheel robot is presented. The balance of the single-wheel robot was intended to be maintained by virtue of the gyroscopic effect induced from a highly rotating flywheel. Since the flywheel rotates at a high speed, an asymmetrical structure of a flywheel causes an irregular rotation and becomes one of the major vibration sources. A vibration was detected and suppressed *a priori* before applying control algorithms to the robot. Gyroscopically induced vibrations can empirically be detected with different rotational velocities. The detection of the balancing angle of the single-wheel robot was accomplished by using an attitude and heading reference system. After identifying the vibrating frequencies, a notch filter was designed to suppress the vibration at the typical frequencies identified through experiments. A digital filter was designed and implemented in a digital signal processor(DSP) along with the control scheme for the balance control performance. The performance of the proposed method was verified by the experimental studies on the balancing control of the single-wheel robot. Experimental results confirmed that the notch filter designed following the detection of the flywheel's vibration actually improved the balancing control performance. A half of the vibration magnitude was reduced by the proposal.

Keywords

Digital notch filter, gyroscopic vibration detection and control, single-wheel robot, attitude and heading reference system sensor

Introduction

Mechanically induced vibrations are always present in dynamical systems, and they are considered as one of the major causes of degrading system performances. Such vibrations even cause instability. Since suppressing vibration is an important task to improve performance, techniques have been investigated for various purposes in industrial systems.

There are usually three steps to address vibration. The first step is to identify the typical frequencies of vibrations using sensors. This is the most important step for suppressing vibrations. Heavily coupled dynamic parts can generate various vibrations. Under these circumstances, it is difficult to precisely identify their true sources, paths, and targets. Therefore, vibration measurement is a challenging problem. Accordingly, filters are designed and implemented in software or hardware on the basis of typical identified frequencies. Finally, control algorithms are applied to satisfy the performance.

For the measurement of vibrations, various techniques are investigated. In Rodrigo et al.,[1] a humidity and vibration measurement sensor system is developed. In Lavatelli and Zappa,[2] a vision-based vibration measurement

Department of Mechatronics Engineering, Chungnam National University, Daejeon, Republic of Korea

Corresponding author:
Seul Jung, Department of Mechatronics Engineering, Chungnam National University, 99 Daehak-ro Yuseong-gu, Daejeon 34134, Republic of Korea.
Email: jungs@cnu.ac.kr

system is proposed. In Hu and Yan,[3] an electrostatic data fusion method is proposed for the simultaneous measurement of belt speed and vibration. In Singh and Sumathi,[4,5] an ultrasonic vibration measurement system is devised for Doppler signal extraction. 3D vibration is measured using a single laser scanning vibrometer in Kim et al.[6] Many different sensing systems have been presented in literature.[7–13] However, in an actual situation, it is difficult to apply the right sensor system in a fully optimized form, and it is also difficult to identify a suitable sensor system for vibration problems.

After measuring vibration, many approaches have been investigated to control vibration problems. Transmitted vibration from vehicles to a driver's body is suppressed by an active force control (AFC) scheme in consideration of the riding convenience. AFC and neuro-AFC schemes are presented to address heavy duty vehicles' vibration problems in Gohari and Tahmasebi.[14] Active noise control (ANC) is designed as an FIR or IIR filter form in the control of an active noise-reducing headrest system in Lei et al.[15] They use a filter as an active controller for noise problems. Active control using an artificial neural network for the gear fault diagnosis in inspecting the state of manufactured gearboxes is presented in Kane and Andhare.[16] In Madhusudana et al.,[17] machine learning is approached in the fault diagnosis problem of face milling cutters. After vibration signals are acquired using an accelerometer mounted on a spindle housing, a diagnosis of face milling tool condition is performed. A non-contact vibration sensing technique is proposed in Hu et al.[18] In Abad et al.,[19] accelerometer sensed vibration is investigated to detect the mechanical fault of an alternator. The vibration mitigation levels (VML) of train-induced ground vibrations are investigated in Younesian and Sadri.[20]

Compared with passive controls such as damper and isolator installation, presently, active control methods have become popular as a state-of-the-art technique. A notch filter technique is applied to reduce the rotating vibration in the motion control system in Hirano et al.[21] Multiple phase-shift notch filters are proposed to suppress the harmonic current of an active magnetic bearing (AMB) rotor system in Cui et al.[22] AMB vibration of CMG-based system by a robust controller is presented in literature.[23–25] The active vibration control for a 'smart' rotor is investigated in van Wingerden et al.[26] Auto-balancing control for a magnetically suspended CMG is proposed where rotor imbalance vibration suppression is considered.[27] An unbalanced induced rotor or asymmetric vibration was detected by sensor fusion in Chaudhury et al.[28]

Therefore, both passive and active isolation techniques are required to become a feasible approach to the given problem. Firstly, the installation of the isolator must be conducted to reject the overall vibration without degrading a sensitive performance. Secondly, the clean signal of the sensor must be confirmed through an active isolation technique. These requirements lead us to investigate extensive experimental studies to characterize the true vibration of the gyroscopic actuator, an investigation on the vibration effect, and verification for the effectiveness of the active isolator.

In this article, a novel approach to solve the vibration problem of a single-wheel robot system (SWR) is presented. Since the SWR uses the gyroscopic effect induced by a high rotating flywheel, resonant vibration frequencies with respect to the rotating velocities of the flywheel are always present. When the highly rotating flywheel is tilted by a gimbal motor, a yawing motion can be generated by means of the gyroscopic effect through the reaction with the friction of the ground.[29,30]

In order to improve the balancing performance of the SWR, the detection of vibrating frequencies is required *a priori*. An attitude and heading reference system (AHRS) sensor is simultaneously used for both the attitude feedback and for the vibration detection. The idea is based on the homogeneity of the mechanism. Indeed, a gyro sensor detects gyroscopic vibrations more accurately. A linear relationship between the flywheel velocities and the frequencies of the vibration is observed through the experimental studies. It was found that the vibrational effect is mainly detected in the yawing rate signals of the sensor system, which is the gyroscopic vibration. After the identification of vibrating frequencies, a notch filter is designed to reduce the vibration. The filter is actually implemented in a DSP in association with the controller. The control performances are verified through the balancing control experiments.

System architecture

The SWR structure is composed of three major components, the controller, the actuator, and the sensor system within a wheel, as shown in Figure 1.

There are three motors inside the wheel, two motors for balancing control and one for driving control. As a main controller, a DSP TMS320F2812 is utilized to control CMG every 10 ms. The control panel transmits the flywheel speed command to the controller through the wireless communication ieee802.15.4. After parsing the command data, the controller sends the command set to the flywheel motor driver NT50A through RS-232C

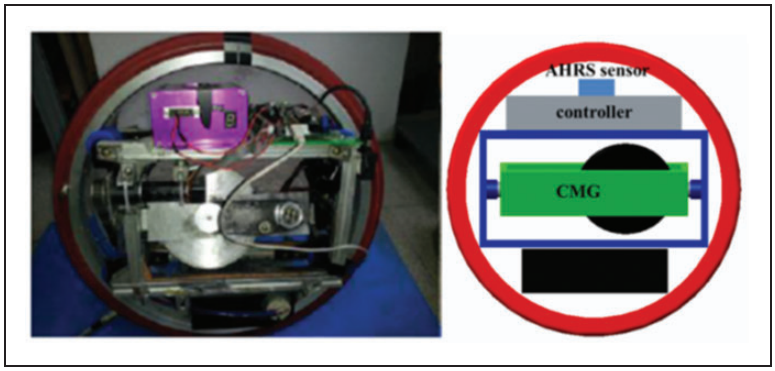

Figure 1. SWR system.

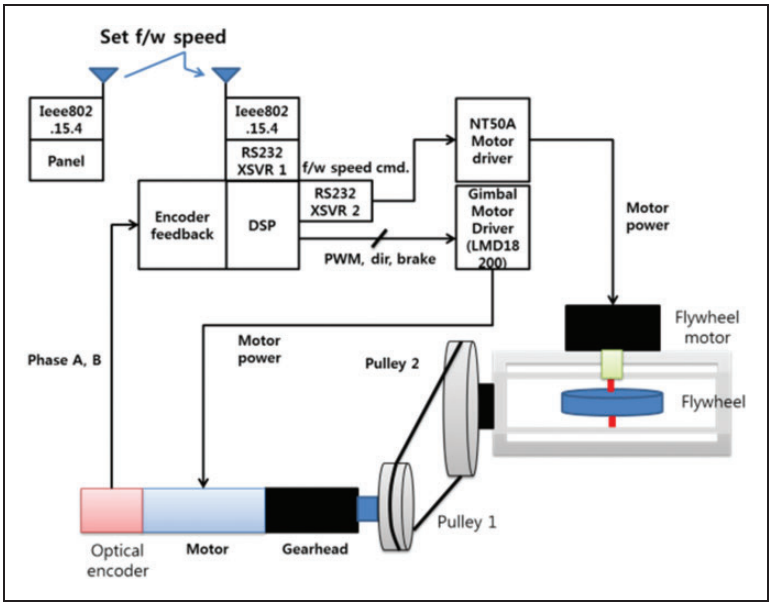

Figure 2. Overall system structure.

communication. The motor driver provides the power to the flywheel motor. The AHRS sensor has a 0.05° resolution and a 100 Hz bandwidth. The control hardware is shown in Figure 2.

Balancing mechanism

The SWR is a self-balancing system that uses a gyroscopic effect induced by a combination of the angular momentum of a flywheel and the tilting rate of a gimbal system, as shown in Figure 3. The tilt motion of the flywheel actually controls the gyroscopic force in the yaw direction. By the reaction effect from the ground friction, the roll motion can be generated.

However, using an asymmetric flywheel structure, unexpected vibrations are easily generated. Although the flywheel is finely manufactured, misalignment with the actuator can cause such a vibrating problem. Therefore, the vibration of a rotating mass is a crucial point in the motion control.

In the given system, the transversal vibration of the flywheel can generate an unexpected tilt motion. A gyroscopic torque can be obtained by the cross product of two vectors as

$$\mathbf{T} = \mathbf{H} \times \boldsymbol{\Omega} \tag{1}$$

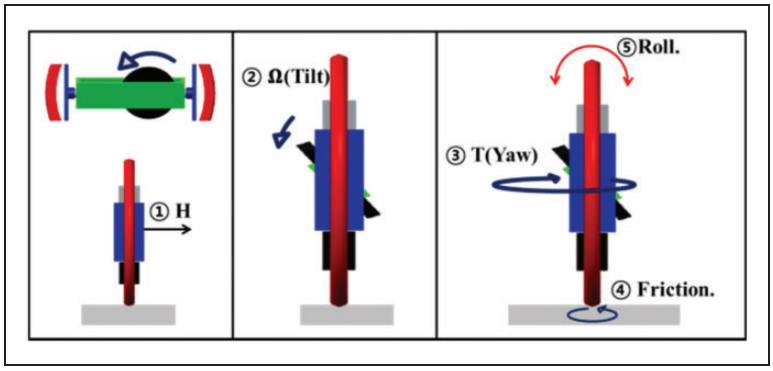

Figure 3. Balancing control mechanism.

where **T** is the gyroscopic vibration torque, **H** is the angular momentum of the flywheel, and **Ω** is the vibrational rate of the flywheel. Therefore, the induced torque direction can easily be changed by the directions of two physical quantities.

The gyroscopic vibration generates the perturbation to the sensed signals. In the feedback control scheme of SWR, the clean measurement is strongly related with the balancing control performance. Although the passive isolation method must be considered in the installation step of the utilized sensor system, it is difficult to satisfy both the sensitivity and the cleanness of the sensor system. The balancing control performance requires sensitive feedback of measured signals as well as the cleanness in the signal. Therefore, investigating the characteristic of the gyroscopic vibration is a first step before applying an active control.

Detection of vibration

In the control of SWR, gyroscopic actuation and sensing process are a principle routine to achieve the balancing performance. For advanced and endurable balancing performance of the robot, sensitive but clean measurement of the attitude is indispensable. To achieve the sensitivity of the utilized sensor, the physical absorber such as passive isolator can be an obstacle in some aspects. Reversely, it is preferable to utilize a dense isolator for the clean measurement. In addition, the proper design of a passive isolator has difficulties due to the space limitation, manufacturing uncertainty, and an installation method. More difficulty of the only-passive isolator method comes in the notch-function design. Although a state-of-the-art technique for the passive isolator design is addressed in Ibrahim[31] and Kamesh et al.,[32] the confirmation of the performance is not mentioned.

The vibrational source of the SWR system originates from the imbalanced flywheel. The speed of the flywheel is controlled as an open-loop manner in the system. Also, the flywheel actuator has no feedback sensor system such as an optical encoder. Only voltage commands are applied to vary the speed of the flywheel in the motor driver. Under this circumstance, direct measurement of the vibrational sources is difficult. In addition, the optimized sensing solution dealing with the gyroscopic sensing is unavailable.

Therefore, our novel idea is to use the same AHRS sensor for the detection of vibrations. Indeed, an AHRS sensor is already utilized for the measurement of a roll angle and a roll angular rate for lateral control of the SWR. The AHRS system consists of three gyro sensors, three accelerometers, and three magnetic sensors inside. The AHRS sensor is implemented by means of the gyroscopic principle. Therefore, it is appropriate for the AHRS sensor to detect gyroscopic vibrations.

To detect the gyroscopic vibration, the experimental setup is described in Figure 4. The ground effect is removed, the panel is used for the speed change of the flywheel, and the data logger is used for logging the sensor data. Since the flywheel motor has no feedback sensor system such as an optical encoder, the flywheel is controlled as an open-loop manner. The speed of the flywheel can be changed by adjusting the steps of the panel. Flywheel motor voltages are tested by increments of 0.2 V and listed in Table 1.

Yaw rate data are gathered with respect to different voltages and are described in Figure 5. The vibrational effects are observed in the yaw rate signals while both the position signals and the acceleration signals are not affected in the measurement. A total of eight steps of yaw rate data are collected, but the vibrational characteristics are hardly seen in the time domain of Figure 5.

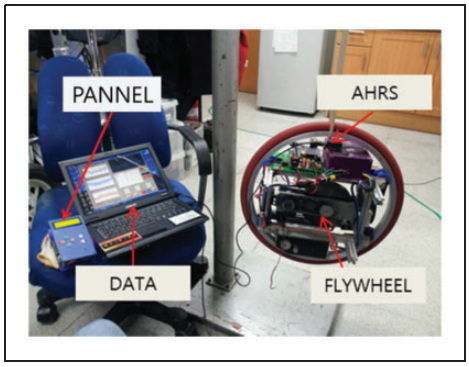

Figure 4. Experimental setup.

Table 1. Flywheel motor voltage.

Steps	Commanded PWM duty ratio (%)	Flywheel motor voltage (V)
(a)	18	2.8
(b)	20	3.0
(c)	22	3.2
(d)	24	3.4
(e)	26	3.6
(f)	28	3.8
(g)	30	4
(h)	32	4.2

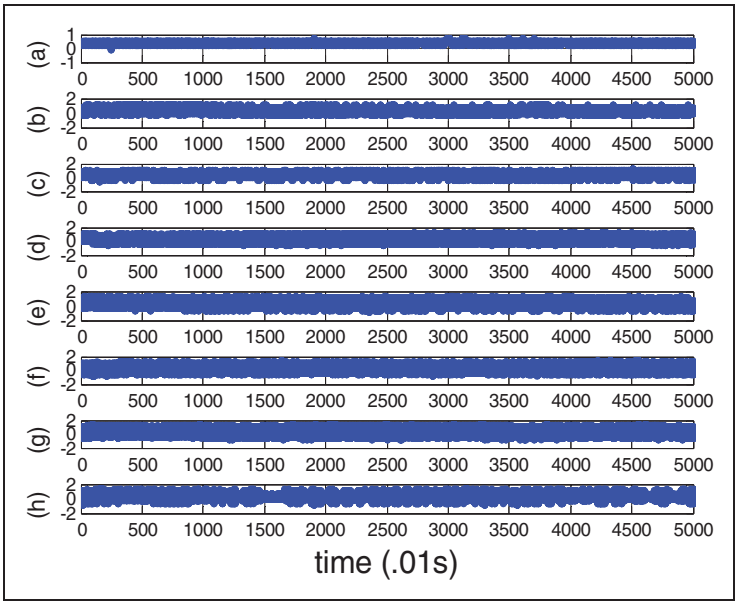

Figure 5. Yaw rate data in the time-domain.

The frequency characteristics of gyroscopic vibrations of Figure 5 are investigated using the FFT (Fast Fourier Transform) and shown in Figure 6. The vibrational frequency peaks appear linearly shifted as the flywheel speeds are linearly increased.

Therefore, there is a linearity between the rotational speed and the gyroscopic vibration. The results show that the gyroscopic vibration can be identified through the speed signals by the AHRS sensor system. In addition, the speed dependency of the gyroscopic vibrations is verified, and the direction of the vibration is clearly shown in the expected yaw motions.

Filter design

The next step is to design a filter to suppress the vibration detected in the experiments. Since our targeted rotational speed is 3517 r/min when duty ratio is 28% and motor voltage is 3.8 V, as indicated in Table 1, the cut off frequency is selected as 42.5 Hz, as shown in Figure 6(f). Therefore, a notch filter is designed to satisfy the specifications, as listed in Table 2.

The prototype of the notch filter can be shown as follows

$$G(s) = \frac{s^2 + \omega^2}{s^2 + bs + \omega^2} \tag{2}$$

where ω represents for the cutoff frequency and coefficient b represents the notch filter bandwidth.

The bilinear transform leads to the resultant filter equations as follows

$$G(z) = \frac{(1+\omega^2) - 2(1-\omega^2)z^{-1} + (1+\omega^2)z^{-2}}{(1+\omega^2+b) - 2(1-\omega^2)z^{-1} + (1+\omega^2-b)z^{-2}} \tag{3}$$

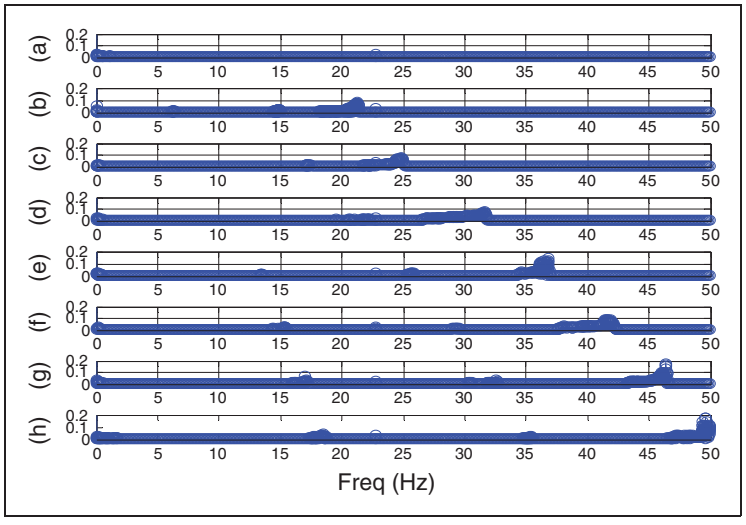

Figure 6. Yaw rate in the frequency-domain.

Table 2. Filter design specifications.

Specification	Value	Unit
Sampling rate	1	Milliseconds
Cutoff frequency	42.5	Hz
Bandwidth	5	Hz

Arranging equation (3) yields

$$G(z) = \frac{1}{2}\frac{\left(z^{-2}+1\right) - 2a_1 z^{-1} + a_2\left(z^{-2}+1\right)}{1 - a_1 z^{-1} + a_2 z^{-2}} \tag{4}$$

where

$$a_1 = \frac{2\cos(\omega T)}{1+\tan(bT/2)},\ a_2 = \frac{1-\tan(bT/2)}{1+\tan(bT/2)}$$

After the coefficients of equation (4) are calculated, the overall transfer function of the digital notch filter can be expressed as follows

$$G(z) = \frac{0.9136 + 1.6281z^{-1} + 0.9136z^{-2}}{1 + 1.6281z^{-1} + 0.8273z^{-2}} \tag{5}$$

The corresponding filter characteristics in the frequency domain are shown in Figure 7.

Control of the vibration

The next step is to suppress the vibration detected in the experiments. When the designed filter is applied, the yaw rate signals are investigated. Figure 8 shows the unfiltered signals and the filtered signals in the time-domain. We clearly see that the magnitude of filtered signals is small. In the time-domain, the mean values of the unfiltered signals and the filtered signals are the same values, 0.3420. However, the covariance of the unfiltered signals is 0.2917 and the covariance of the filtered signals is 0.873.

Figure 9 shows the unfiltered signals and the filtered signals in the frequency domain. It is clearer in the frequency domain that signals around 42.5 Hz appear to be large, as illustrated in Figure 9(f). Those signals are reduced after filtering, as shown in Figure 9(f). We clearly see that signals at 42.5 Hz are filtered out.

In the power spectrum, the filtering power and the filtered power are compared in Figure 10. The unexpected vibration of −10 dB reduction has been achieved by the designed notch filter.

Experiment

For experimental verification, the designed notch filter is added to the control algorithm.

The overall control scheme is shown in Figure 11. The primary control is a PD control method along with the filtering technique. The PD control torque can be calculated as

$$\tau = K_p\theta_e + K_d\dot{\theta}_e - K\dot{\theta}_{fy} \tag{6}$$

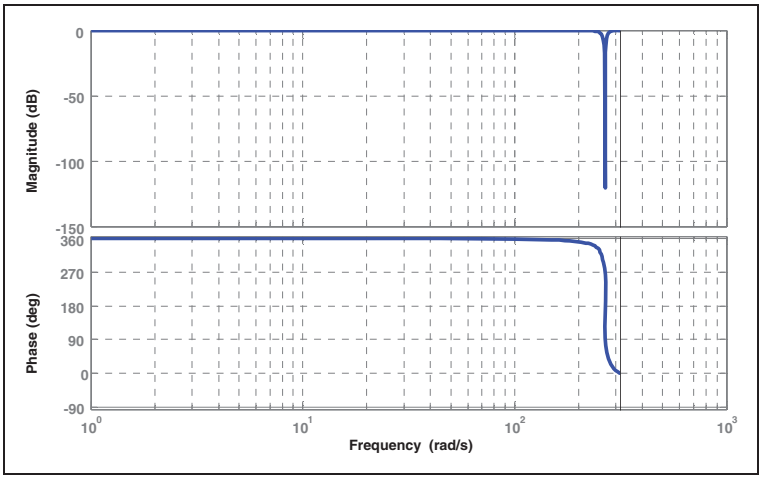

Figure 7. Notch filter characteristics.

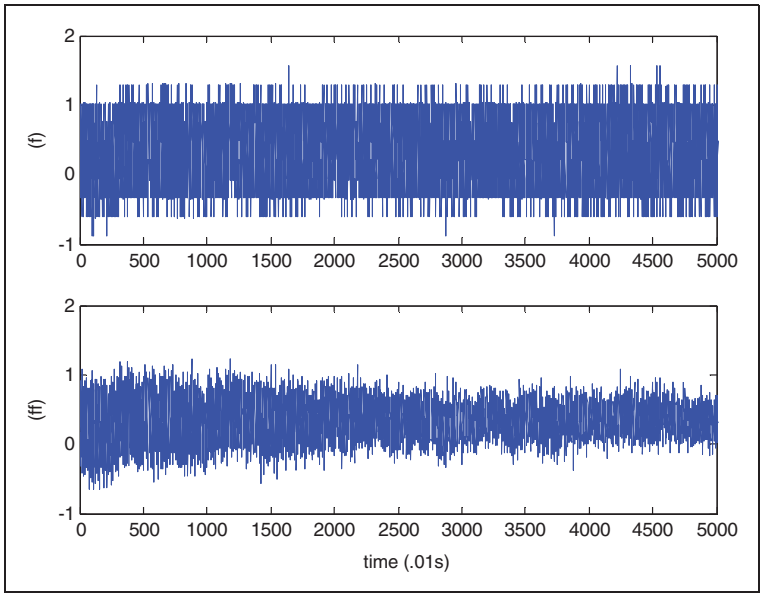

Figure 8. Notch filter effect in time-domain: (f) unfiltered data, (ff) the filtered data.

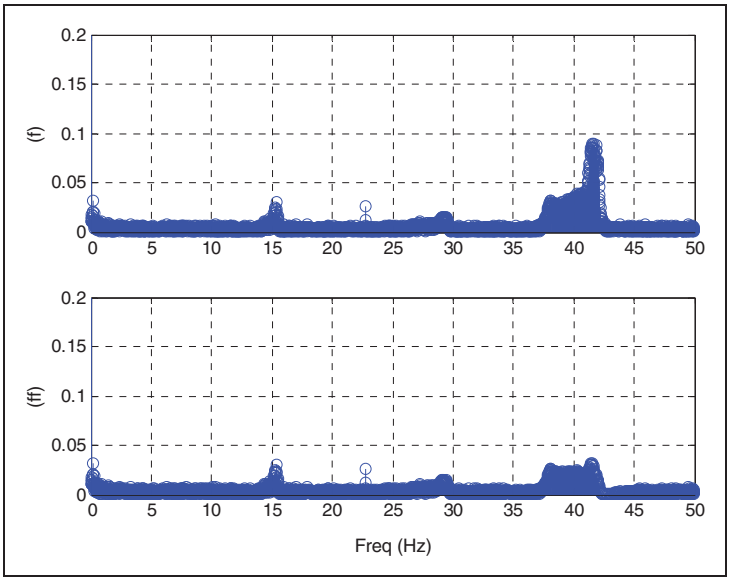

Figure 9. Notch filter effect in frequency-domain: (f) the unfiltered signal, (ff) the filtered signal.

where θ_d is the desired angle, $\dot{\theta}_d$ is the desired angular rate, θ_e is angle error, $\dot{\theta}_e$ is the error rate, θ_f is angle feedback, $\dot{\theta}_f$ is the feedback rate, $\dot{\theta}_y$ is the yaw rate, and $\dot{\theta}_{fy}$ is the filtered yaw rate. Controller gains are found empirically that K_p is 1050, K_d is 50, and K is 12. V_{in} is the motor driver input voltage, and τ is the torque input. The designed notch filter is implemented in the DSP.

The experimental setup is shown in Figure 12. The SWR is initially located on the reference line marked on the floor in order to distinguish the deviation due to the vibration.

To evaluate the balancing control performances of the SWR system, 10 identical experiments are conducted. Among them, three successful results are plotted for 250 s in Figure 13. The mean, variance, and RMS error for the three cases are listed in Table 3. The deviation from the reference is about 5°, which means the oscillatory balancing response although the balancing control was successful.

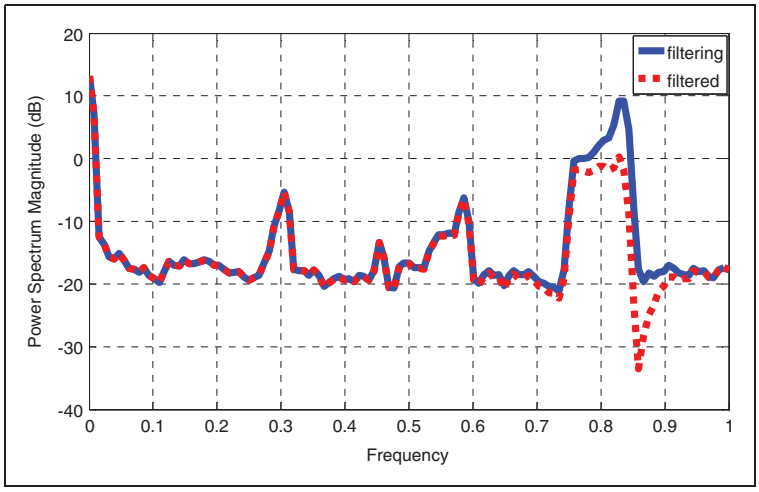

Figure 10. Power spectrum comparison.

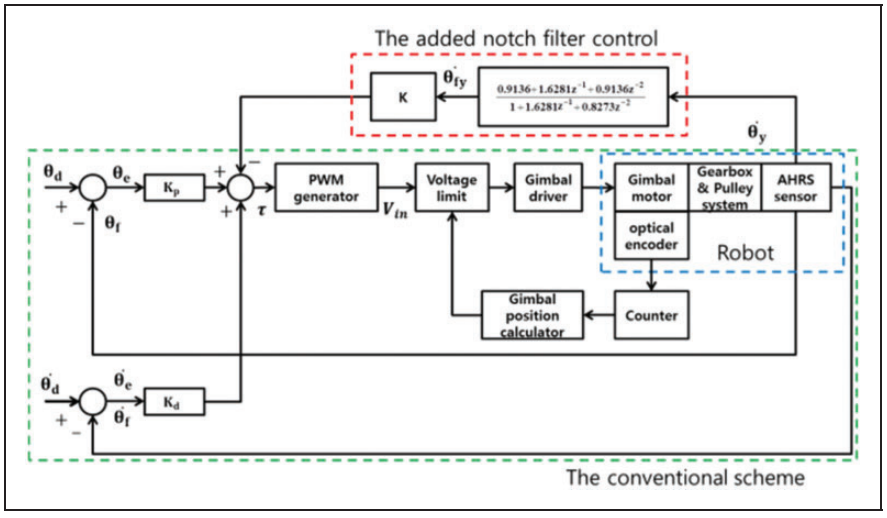

Figure 11. The proposed control scheme.

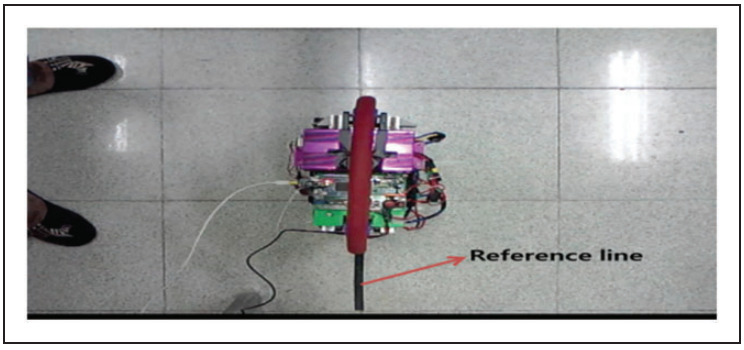

Figure 12. Experimental setup (top view).

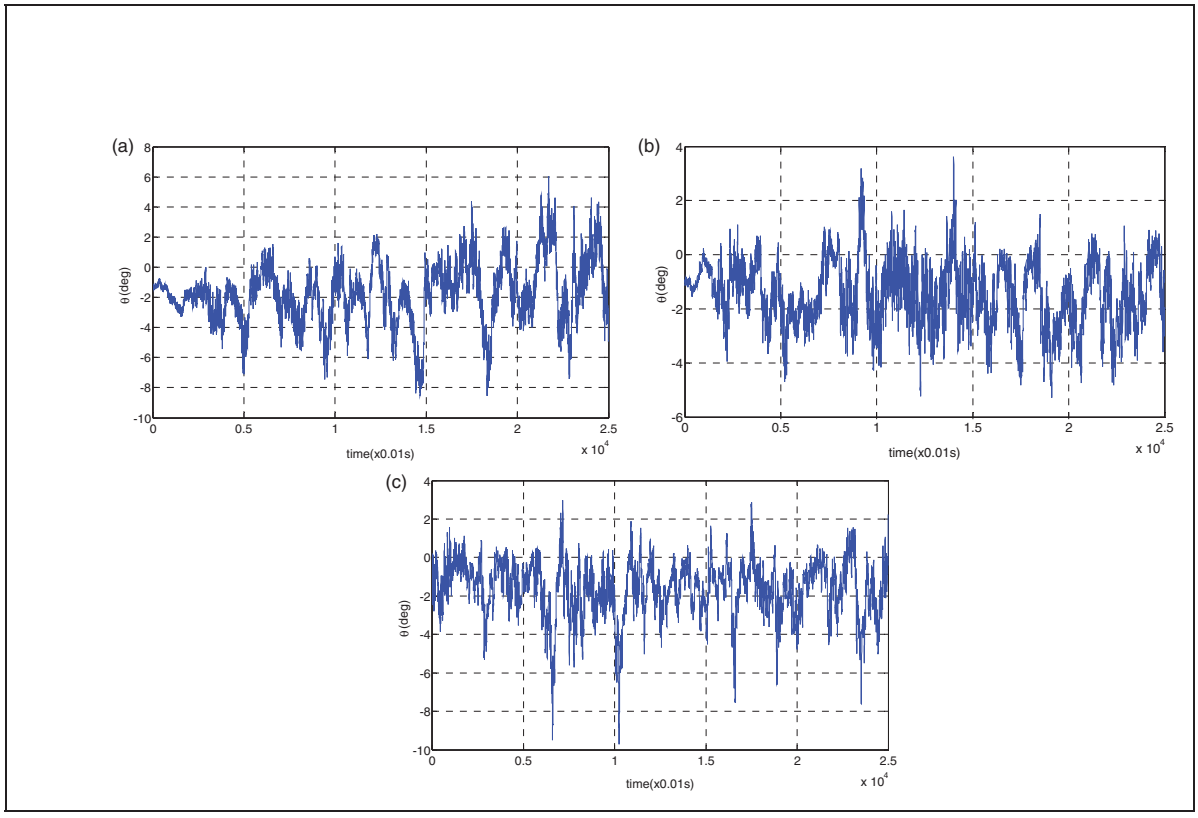

Figure 13. PD-only control performances.

Table 3. PD control balancing performances.

Tasks	Mean	RMSE	Std.
Task 1	−1.7271	328.8048	2.0796
Task 2	−2.8321	190.8433	1.2070
Task 3	−2.3736	231.8297	1.4662

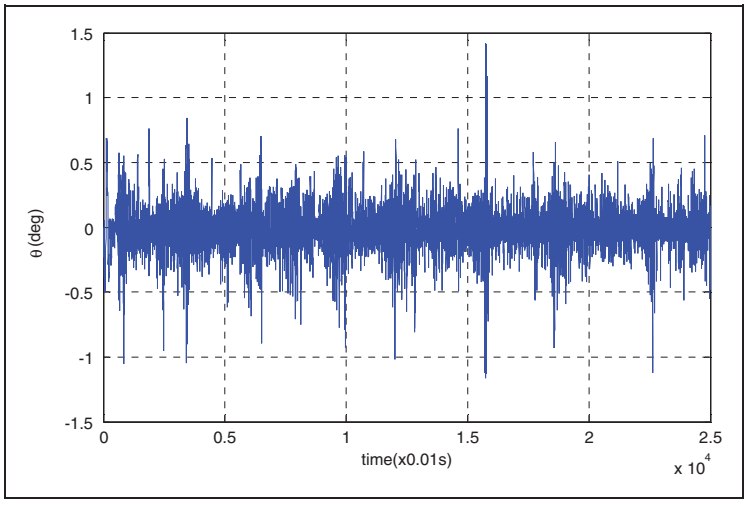

Figure 14. Control performance with filter.

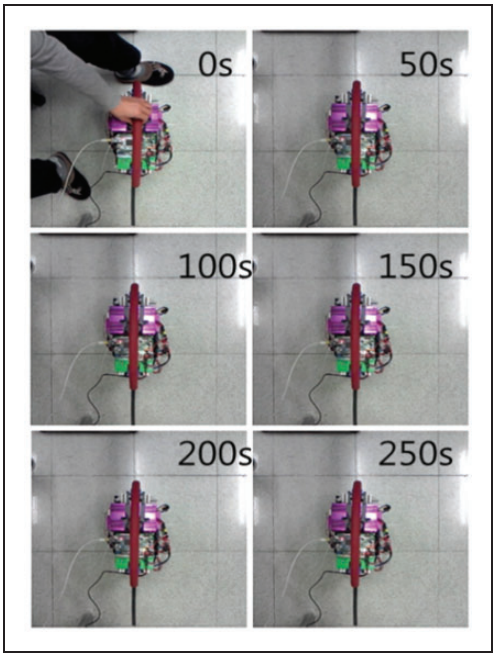

Figure 15. Balancing control performance.

Table 4. Balancing control performance.

Items	Mean	RMSE	Std.
Roll angle	−0.0090	25.4510	0.1610

Next, we add the filtering technique to the controller and perform the same experiment. The balancing performance, displayed in Figure 14, shows a much smaller deviated error, namely 1°. It is clear that filtering the vibration improves the balancing performance of the SWR considerably. The corresponding captured video images are shown for 250 s in Figure 15.

When balancing angle errors are compared between Tables 3 and 4, we clearly see that the error for the filtering case is much smaller than that without a filter. The deviation error of the SWR from the reference line is much smaller, and the vibration has been suppressed.

Conclusion

The balancing control performance of the SWR depends upon the gyroscopic force induced from the fast rotating flywheel, which causes vibration. The gyroscopically induced vibration has been managed by identifying by an AHRS sensor and by filtering the vibration frequency by the notch filter. The vibration has been remarkably reduced and the balancing performance of the SWR has been improved. It is also confirmed that an AHRS sensor can be used as a measurement device as well as utilized for measuring the attitude of the system. Therefore, when typical sensors are unavailable, an AHRS sensor could be one optimal sensor for detecting vibration of the system.

Declaration of conflicting interests

The author(s) declared no potential conflicts of interest with respect to the research, authorship, and/or publication of this article.

Funding

The author(s) disclosed receipt of the following financial support for the research, authorship, and/or publication of this article: This research has been supported by the National Research Foundation of Korea under the contract of NRF-2014R1A2A1A11049503 and 2016R1A2B2012031)

References

1. Rodrigo SR, Aldaba AL, Herrera RAP, et al. Simultaneous measurement of humidity and vibration based on a microwire sensor system using fast Fourier transform technique. *J Lightwave Technol* 2016; 34: 4525–4530.
2. Lavatelli A and Zappa E. Modeling uncertainty for a vision system applied to vibration measurements. *IEEE Transac Instrument Measure* 2016; 65: 1818–1826.
3. Hu Y and Yan Y. Simultaneous measurement of belt speed and vibration through electrostatic sensing and data fusion. *IEEE Transac Instrument Measure* 2016; 65: 1130–1138.
4. Singh KM and Sumathi P. Synchronization technique for Doppler signal extraction in ultrasonic vibration measurement systems. *IEEE Transac Instrument Measure* 2015; 6: 3162–3172.
5. Singh KM and Sumathi P. Vibration parameter estimation methods for ultrasonic measurement systems – a review. *IET Sci Measure Technol* 2015; 9: 492–504.
6. Kim D, Song H, Khalil H, et al. 3-D vibration measurement using a single laser scanning vibrometer by moving to three different locations. *IEEE Transac Instrument Measure* 2014; 63: 2028–2033.
7. Nishino ZT, Chen K and Gupta N. Power modulation-based optical sensor for high-sensitivity vibration measurements. *IEEE Sens J* 2014; 14: 2153–2158.
8. Sun XT, Jing XJ, Xu J, et al. A quasi-zero-stiffness-based sensor system in vibration measurement. *IEEE Transac Ind Electron* 2014; 61: 5606–5614.
9. Dreier F, Gunther P, Pfister T, et al. Interferometric sensor system for blade vibration measurements in turbomachine applications. *IEEE Transac Instrument Measure* 2013; 62: 2297–2302.
10. Addabbo T, Fort A, Biondi R, et al. Measurement of angular vibrations in rotating shafts: effects of the measurement setup nonidealities. *IEEE Transac Instrument Measure* 2013; 62: 532–543.
11. DeShaw J and Rahmatalla S. Comprehensive measurement in whole-body vibration. *J Low Frequency Noise Vib Active Control* 2012; 31: 63–74.
12. Nabhan A, Nouby M, Sami AM, et al. Vibration analysis of deep groove ball bearing with outer race defect using ABAQUS. *J Low Frequency Noise Vib Active Control* 2016; 35: 1–14.
13. Yang SM and Wang SC. The detection of resonance frequency in motion control systems. *IEEE Transac Ind Applicat* 2014; 50: 3423–3427.
14. Gohari M and Tahmasebi M. Active off-road seat suspension system using intelligent active force control. *Journal Low Frequency Noise Vib Active Control* 2015; 34: 475–490.
15. Lei C, Xu J, Wang J, et al. Active headrest with robust performance against head movement. *J Low Frequency Noise Vib Active Control* 2015; 34: 233–250.
16. Kane PV and Andhare AB. Application of psychoacoustics for gear fault diagnosis using artificial neural network. *J Low Frequency Noise Vib Active Control* 2016; 35: 207–220.
17. Madhusudana CK, Budati N, Gangadhar HK, et al. Fault diagnosis studies of face milling cutter using machine learning approach. *J Low Frequency Noise Vib Active Control* 2016; 35: 128–138.
18. Hu Y, Yan Y, Wang L, et al. Non-contact vibration monitoring of power transmission belts through electrostatic sensing. *IEEE Sens J* 2016; 16: 3541–3550.
19. Abad M, Moosavian A and Khazaee M. Wavelet transform and least square support vector machine for mechanical fault detection of an alternator using vibration signal. *J Low Frequency Noise Vib Active Control* 2016; 35: 52–63.
20. Younesian D and Sadri M. Performance analysis of multiple trenches in train-induced wave mitigation. *J Low Frequency Noise Vib Active Control* 2014; 33: 47–64.
21. Hirano K, Nishimura S and Mitra SK. Design of digital notch filters. *IEE Transac Commun* 1974; 22: 964–970.
22. Cui P, Li S, Wang Q, et al. Harmonic current suppression of an AMB rotor system at variable rotation speed based on multiple phase-shift notch filters. *IEEE Transac Ind Electron* 2016; 63: 6962–6969.
23. Fang J, Zheng S and Han B. AMB vibration control for structural resonance of double-gimbal control moment gyro with high-speed magnetically suspended rotor. *IEEE Transac Mechatron* 2013; 18: 32–43.
24. Chen Q, Liu G and Han B. Suppression of imbalance vibration in AMB-rotor systems using adaptive frequency estimator. *IEEE Transac Ind Electron* 2015; 62: 7696–7705.
25. Liu C and Liu G. Field dynamic balancing for rigid rotor-AMB system in a magnetically suspended flywheel. *IEEE/ASME Transac Mechatron* 2016; 21: 1140–1150.
26. Van Wingerden JW, Hulskamp A, Barlas T, et al. ''Two-degree-of-freedom active vibration control of a prototyped ''Smart'' rotor''. *IEEE Transac Control Syst Technol* 2010; 19: 284–296.
27. Liu Cand Liu G. Autobalancing control for MSCMG based on sliding-mode observer and adaptive compensation. *IEEE Transac Ind Electron* 2016; 63: 4346–4356.
28. Chaudhury SB, Sengupta M and Mukherjee K. Experimental study of induction motor misalignment and its online detection through data fusion. *IET Electric Power Appl* 2012; 7: 58–67.
29. Zhu Y, Gao Y, Xu C, et al. Adaptive control of a gyroscopically stabilized pendulum and its application to a single-wheel pendulum robot. *IEEE Transac Mechatron* 2015; 20: 2095–2106.

30. Lee SD and Jung S. Experimental verification of stability region of balancing a single-wheel robot: an inverted stick model approach. *IECON* 2015; 4556–4561.
31. Ibrahim RA. Recent advances in nonlinear passive vibration isolators. *J Sound Vib* 2008; 314: 371–452.
32. Kamesh D, Pandiyan R and Ghosal A. Modeling, design and analysis of low frequency platform for attenuating micro-vibration in spacecraft. *J Sound Vib* 2010; 329: 3431–3450.